Acta Scientiarum

http://www.uem.br/acta
ISSN printed: 1806-2563
ISSN on-line: 1807-8664
Doi: 10.4025/actascitechnol.v39i4.29904

Energetic analysis of a commercial absorption refrigeration unit using an ammonia-water mixture

Josegil Jorge Pereira de Araújo[1,2,3], Carlos Antônio Cabral dos Santos[2,6], Carlos Almir Monteiro de Holanda[4], João Batista Furlan Duarte[4], Alvaro Antonio Ochoa Villa[5,6*] and José Carlos Charamba Dutra[6]

*[1]Universidade Federal de Sergipe, São Cristóvão, Sergipe, Brazil. [2]Universidade Federal da Paraíba, João Pessoa, Paraíba, Brazil. [3]Universidade de Fortaleza, Fortaleza, Ceará, Brazil. [4]Universidade Federal do Ceará, Fortaleza, Ceará, Brazil. [5]Instituto Federal de Tecnologia de Pernambuco, Avenida Professor Luiz Freire, 500, 50740-540, Recife, Pernambuco, Brazil. [6]Universidade Federal de Pernambuco, Avenida Professor Moraes Rego, 1235, 50670-901, Recife, Pernambuco, Brazil. *Author for correspondence. E-mail: ochoaalvaro@recife.ifpe.edu.br*

ABSTRACT. The ROBUR® absorption refrigeration system (ARS), model ACF60, with a capacity of 17.5 kW, is tested, modeled and simulated in the steady state. To simulate the thermal load a heating system with secondary coolant was used, in which a programmable logic controller (PLC) kept the inlet temperature EVA at around 285.15 K. The mathematical model used was based on balancing the mass, energy and ammonia concentrations and completed by closing equations such as, Newton's cooling equation. The mathematical model was implemented using the Engineering Equation Solver – EES®. The results obtained after modeling and a numerical permanent simulation are studied using the Duhring diagram. Potential points of internal heat recovery are visualized, and by using graphs of the binary mixture, it is possible to identify the thermodynamic states of all monitored points. The data obtained in the numerical simulation of the ARS was compared with data acquired in the actual tests of the ARS with the ROBUR® apparatus.

Keywords: air conditioning, absorption system, simulation, experimental results, COP.

Análise energética de um chiller de refrigeração por absorção comercial utilizando a mistura amônia-água

RESUMO. O sistema de refrigeração por absorção (SRA) da ROBUR®, modelo ACF60, com capacidade de 17,5 kW, foi testado, modelado e simulado em regime permanente. Para simular a carga térmica um sistema de aquecimento com refrigerante secundário foi utilizado, e através de um controlador programável lógico (CLP) foi mantida a temperatura de entrada da água no evaporador ao redor de 285,15 K. O modelo matemático foi baseado nas equações de balanço de massa, energia e concentração de amônia, e completado pelas equações de fechamento, tais como, a equação de resfriamento de Newton. O modelo matemático foi implementado no *Engineering Equation Solver - EES®*. Os resultados obtidos com a modelagem e simulação numérica permanente são estudados usando o diagrama de Duhring. Potenciais pontos de recuperação de calor interno são visualizados. Os pontos de estados termodinâmicos monitorados são visualizados com os gráficos de mistura binária. Os dados obtidos nas simulações numéricas do SRA foram comparados com os obtidos nos testes reais do sistema com o chiller ROBUR®.

Palavras-chave: ar condicionado, sistema de absorção, simulação, resultados experimentais, COP.

Introduction

One of the major problems in the refrigeration field is how best to control air conditions or processes by controlling the temperature and humidity in order to achieve optimum comfort conditions or processes. Cooling equipment is used to achieve comfort temperatures in air conditioning applications, or operating temperatures in manufacturing processes. These items of equipment are available in various technologies, vapor compression being the one that is most used in refrigeration systems, and for which electric energy drives the mechanical compressor. A technology that has already been much used is the Absorption Refrigeration System (ARS), where heat is the energy source (Kohlenbach & Ziegler, 2008a, 2008b, Rodriguez-Muñoz & Belman-Flores, 2014). The interest in using the ARS is related to shortages of electric energy. If the cost of producing this energy increases, ARSs would be manufactured, and, otherwise, if the cost decreases, the interest in manufacturing these systems decreases (Wu, Wang,

Shi, & Li, 2014; Rivera, Best, Cardoso, & Romero, 2015; Wu, Shi, Li, & Wang, 2015).

An ARS basically consists of the following items: generator, condenser, expansion valve, evaporator, absorber, reducing valve and a solution pump. A feature of absorption systems is that they use a refrigerant mixture as a working fluid. Generally, two substances are involved, one of which works as a refrigerant fluid and the other as an absorber. Several mixtures are used as working fluids, e.g., ammonia/water, water/lithium bromide, water/sulfuric acid, ammonia/sulfocyanide; ammonia lithium/nitrate (Libotean, Salavera, Valles, Esteve, & Coronas, 2007; Amaris, Bourouis, Vallès, Salavera, & Coronas, 2014).

Modeling and numerical simulation are widely used to predict the behavior and efficiency of ARSs as a single component (Rabah, 2010; Somers et al., 2011; Ochoa, Dutra, Henríquez, & Santos, 2016), as well as in cogeneration systems (Moya et al., 2011; Ochoa, Dutra, Henríquez, & Rohatgi, 2014) and solar energy systems (Edem, Le Pierrès, & Luo, 2012; Ozgoren, Bilgili, & Babayigit, 2012).

In this context, the study by Kim and Park (2007) developed a dynamic model of a commercial absorption chiller of 3 RT cooling capacity using the pair NH_3/H_2O, the aim of which was to find a control strategy configuration that enables the chiller to perform better due to the flow rate of the concentration and solution. Darwish, Al-Hashimi, and Al-Mansoori (2008) performed an analysis of an ARS manufactured by ROBUR®, using the Aspen Plus Flowsheet Simulator, and found the coefficient of performance (COP) was improved by up to 20%, when a throttling process was introduced directly before the separator, and Ochoa, Dutra, and Henríquez (2014) developed a theoretical model of an $LiBr/H_2O$ absorption chiller based on the First and Second Laws of Thermodynamics where the analysis revealed that the main instances of irreversibility were found in the cooling tower, generator and absorber, with values of 34, 32 and 16% respectively while the values for the energy and exergy COP of the system were 0.74 and 0.24, respectively. Boudéhenn et al. (2012) presented a numerical and experimental analysis of the prototype of an NH_3/H_2O absorption chiller for solar cooling applications with 5 kW cooling capacity, where the COP of the system was around 0.60. Lin, Wang, and Xia (2011) conducted an investigation on the feasibility of a two-stage air-cooled ammonia/water absorption refrigeration system, and verified that thermal COP is 0.34 and electrical COP is 26 under typical summer conditions using 85°C hot water supplied from a solar collector. Many experimental studies have been conducted on absorption chillers using the pair NH_3/H_2O (Beccali, Cellura, Longo, Nocke, & Finocchiaro, 2012; Said et al., 2015; Zotter & Rieberer, 2015).

A numerical-experimental analysis on an NH_3/H_2O refrigeration absorption chiller with 10 kW cooling capacity was conducted by (Le Lostec, Galanis, & Millette, 2012, 2013), in which the performance of the absorption chiller decreased significantly when the temperature of the evaporator decreased. In the same context, but using different working fluids, Wu, Wu, Yu, Zhao, and Wu (2011) compared the use of binary and of ternary solutions on a new, ammonia absorption chiller that used solar energy as the driving source. The results showed that the COP of the chiller when using the ternary solution was almost 40% higher than those using the binary solution. The concept of hybrid refrigeration systems has been used to increase the performance of a chiller. This is done by combining the configuration of compression and absorption. This increases the heat and mass transfer which enables the overall performance of these systems to be improved. In this context, Pratihar, Kaushik, and Agarwal (2012) presented an evaluation of a small capacity absorption/compression refrigeration system so as to investigate the performance of the absorber and generator (heat exchanger) on the COP and the cooling capacity of the system.

The development of their work was divided into three stages: 1) modeling and simulating the ARS in the steady state; 2) testing a commercial ARS and, 3) comparing the data obtained with numerical simulations and tests made with the ARS. In the ARS simulation, the following were calculated: temperature, enthalpy, concentration and pressure at each point of state. The heat flows were calculated and, consequently, the coefficient of performance, COP, of the ROBUR® unit. In the comparative analysis the temperatures of the points of state obtained from steady state simulations were matched with those obtained from the ARS test.

Material and methods

This Section is divided into three parts: The ROBUR cooling system by absorption; experimental analysis; and the mathematical formulation of the ARS.

The ROBUR® cooling system by absorption

The ROBUR® ARS is an absorption refrigeration system of simple effect, using an

ammonia and water solution as the working fluid. This system comprises the following components: generator (GERA), rectifier (RET), condenser (COND), concentric heat exchanger (HEC), evaporator (EVA), absorber (ABS), absorber - air heat exchanger (AHEA), solution pump (SP) and three pressure reduction valves (RV), as depicted in Figure 1.

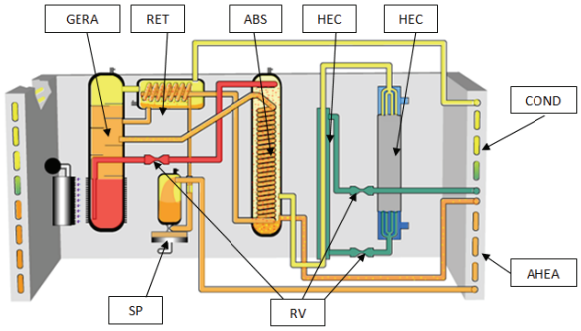

Figure 1. Schematic Diagram of the Robur ARS (ROBUR®).

The ARS has three levels of pressure: the highest level contemplates the following components: GERA, RET, coil of the rectifier (CRET), coil of the absorber (CABS) and COND; the intermediate level, where the liquid flows in the HEC, in the annular space; and the lower level, where one finds the EVA, steam flowing in the HEC along its tube side, the ABS and the AHEA.

Three different streams are found in the system: the first, with the flow of absorbent, comprising a solution of ammonia-water, the concentration of which is modified in the GERA and in the ABS. The second flow of absorbent occurs in the following components: GERA, pressure reducing valve (RV3), ABS, AHEA, SP, CRET, CABS; the second, with the ammonia flow which has a small concentration of water (primary coolant). This occurs in the following components: the top of GERA, RET, COND, RV1, HEC, EVA and ABS; the third is the flow of water which will be refrigerated in the EVA, i.e., the secondary fluid of refrigeration.

The heat flux entering the GERA, coming from the burning of a fossil fuel - LPG (Liquefied Petroleum Gas) - activates the system. With the energy gain, ammonia, being more volatile, vaporizes from the solution and flows to the RET. Together with the ammonia vapor, there is steam, but only in small quantity. In the countercurrent, a downward flow of strong solution of ammonia-water enters at the top of the GERA, promoting a heat exchange between flows, resulting in condensation of a small amount of steam and ammonia, thereby purifying the ammonia-water solution. The mixture in the vapor phase leaves the GERA and flows towards RET in a slightly overheated state. In the RET, the solution is cooled, thus prompting more condensation for the steam part, and therefore making the ammonia solution even purer. The heat is transferred from the shell side of the RET to the inner coil of the CRET, through which the strong liquid solution flows. The portion of condensed water returns to the GERA. It is worth emphasizing that this purification is necessary to reduce the amount of water vapor that flows to the EVA because the accumulation of water in the EVA reduces the efficiency of the whole system.

The mixture in the slightly superheated vapor state flows to the COND, exchanges heat with the outside air, thus causing the mixture to condense. At the exit of the COND, the solution of ammonia-water is a saturated liquid and its pressure is reduced to the intermediate level of pressure in RV1. From RV1, the solution flows to the HEC, passing through the annular, and transfers heat to the fluid flowing in the inner part of the central tube. On leaving the HEC, the pressure of the subcooled liquid solution is reduced in RV2 to the temperature and pressure of the evaporation. In the EVA, heat is exchanged between the solution and the secondary cooling fluid water, resulting in evaporation of the solution along the EVA. On leaving the EVA as saturated vapor, the mixture flows to the HEC, in its central tube, and exchanges heat with the liquid solution flowing in the annular space. The vapor stream then leaves the HECA superheated vapor, and enters the ABS. There it will initiate a process of ammonia absorption with the weak ammonia-water solution coming from the GERA. In this process, heat is liberated, a characteristic of an exothermic reaction. This heat of the reaction is transferred from the system by recovering internal heat as in the case of the ABS coil (CABS), and is still expelled into the environment in AHEA. In the recovery of internal heat, a fuel economy is achieved because the solution comes with a higher temperature in GERA, thus decreasing the amount of fuel necessary to achieve the final operating temperature. The absorption process is completed in AHEA, when the heat of the reaction is transferred to the outside environment, which is at ambient temperature.

The weak solution that leaves the GERA to ABS, before passing through the coil of the GERA (not depicted in Figure 1), then undergoes throttling in RV3, causing the pressure to drop to its lowest level. At the end of the absorption process in the AHEA, the solution in liquid state flows to the SP. This pump has two biases in the ARS: the first, which

causes the movement of liquid within the heat exchangers, thus making an increased heat and mass transfer possible, and secondly, the liquid solution of the low side pressure is transported to the high side pressure, causing the liquid to be mixed inside the GERA (Herold, Radermacher, & Klein, 1996). However, before entering the GERA, the solution passes through two heat exchangers, the CRET and the CABS, both of which were described above. With the entry of the strong solution as subcooled liquid in the GERA, one returns to the initial point of a new cycle. Figure 2 shows the schematic of the ARS, with all of the control volumes and the eighteen points of thermodynamic state for the modeling and simulation in the steady state regime.

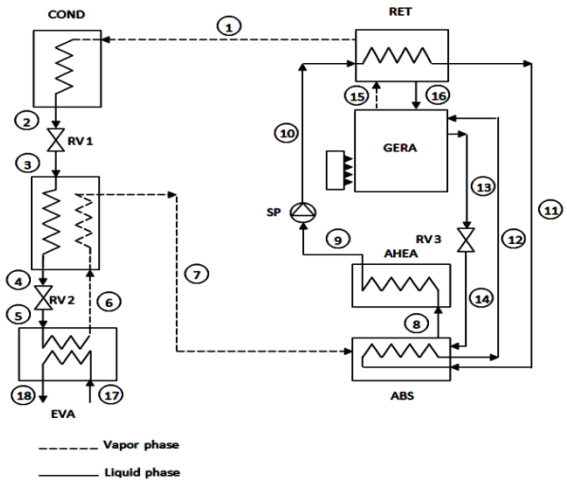

Figure 2. Schematics of the ARS, with all the control volumes and the eighteen points of thermodynamic state for the modeling and simulation in steady state regime (Herold et al., 1996).

Experimental analysis of the ROBUR® ARS

To study the operation of a ROBUR® ARS, a system was assembled to simulate the determination of the thermal load. Figure 3 shows a diagram of the installation, with the circuit of the secondary coolant. The reason for the water reservoir is to maintain a constant water supply to the pump. The boiler of the system was constructed using 1,020 steel tubes which were 0.15 m diameter and 1 m in length. An electric 18 kW resistance heater is assembled at one of end of the apparatus.

The data acquisition system data Taker DT800 was used to read the temperatures which were then stored by the communication software DT800-Friendly. To maintain the EVA inlet temperature around 285.15 K, a programmable logic controller (PLC) was used, thus providing a proportional integral and derivative control (PID).

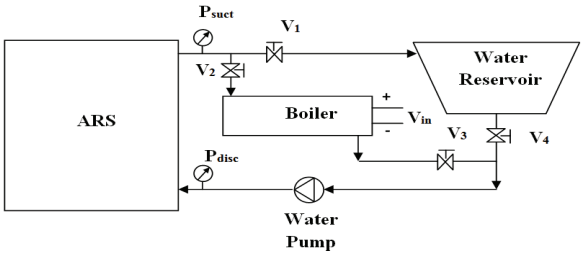

Figure 3. Installation diagram of the ROBUR® ARS.

A centrifugal pump keeps the water circulating in the chiller, the pressure being controlled by a water valve. The discharge pressure (P_{disc}) of the circulating water is maintained at 2.5 kgf cm^{-2} and the suction (P_{suct}) at 1.2 kgf cm^{-2}. The sixteen points of the ARS were monitored so as to analyze the ARS temperatures and one point was installed so as to measure the ambient temperature. The test was initiated when the temperatures were stabilized at the ambient air temperature. The equipment was run for sixty minutes.

Mathematical formulation

The ARS depicted in Figure 1 and 2 was divided into several control volumes which represent the 'units' which comprise the system. Each of the control volumes has an inlet and outlet point, the properties of which were calculated to define the thermodynamic state of each one. Balance equations will be applied in each of the control volumes, thereby obtaining a system of equations to solve the problem. Complementary equations were used to solve the system of equations, which required some assumptions to be made: 1) the system operates in the steady state, with mass conservation; 2) pressure drops in the pipes were considered as negligible; 3) the contribution of kinetic and potential energies were considered as negligible in all control volumes; 4) heat exchanges to the surroundings were considered very low for all components, except in COND and AHEA; 5) expansions in pressure-reducing valves were considered isenthalpic; 6) material flows entering and leaving the apparatus were considered as being one-dimensional.

The system was modeled using material balance for the ammonia/water solution; concentration balance for the ammonia species; and energy balance around the system. The material balance equation is given by the Equation 1:

$$\sum_{in} \dot{m}_{in} = \sum_{out} \dot{m}_{out} \quad (1)$$

where:

$\dot{m}$ is the mass flow rate. The *in* and *out* subscripts represent the inlet and outlet of the control volume, respectively.

The balance equation for concentration of ammonia species is given by Equation 2:

$$\sum_{in} \dot{m}_{in} C_{in} = \sum_{out} \dot{m}_{out}\, C_{out} \quad (2)$$

where:
C is the concentration of ammonia.

For the energy balance equation, the contributions of kinetic and potential energies were considered, so it can be written as Equation 3:

$$\dot{Q}_{cv} + \sum_{in} \dot{m}_{in} i_{in} = \dot{W}_{cv} + \sum_{out} \dot{m}_{out} i_{out} \quad (3)$$

where:
$\dot{Q}_{cv}$ is the heat rate in control volume;
i is the specific enthalpy;
$\dot{W}_{cv}$is the work rate that crosses the boundaries of the control volume.

To complement the set of equations, closing equations were necessary. Some of these Equation 4 and 5 are:

a) The sum of concentrations of ammonia and water:

$$C_{NH3} + C_{H2O} = 1 \quad (4)$$

b) The heat rate in components such as HEC, CRET and ABS:

$$\dot{Q}_{cv} = \dot{m}_{cv} cp_{cv} (T_{in} - T_{out}) \quad (5)$$

where:
c_p is the specific heat at constant pressure,
T is the temperature.

c) In calculating the work rate over the SP, the pumping process was considered as isentropic, isochoric and adiabatic, the work rate being calculated by Equation 6:

$$W_{cv} = \frac{v \cdot \dot{m}_{in}}{\eta_{pump}} \left(P_{high} - P_{low}\right) \quad (6)$$

where:
v is the specific volume of liquid at the pump inlet;
$\dot{m}_{in}$is the mass flow rate;
η_{pump} is the pump efficiency and P_{high} and P_{low} are, respectively, the pressures of high and low of the system. In determining pressure levels, the study by Bourseau and Bugarel (1986) has been considered, wherein the pressure value is determined by the following Equation 7:

$$\log(p) = A - \frac{B}{T} \quad (7)$$

where:
T is the condensation temperature for the high side or the evaporation temperature for the low side, *A* and *B* are parameters that must be determined by Equation 8 and 9, respectively:

$$A = 7.44 - 1.767 \cdot C + 0.9823 \cdot C^2 + 0.3627 \cdot C^3 \quad (8)$$
$$B = 2013.8 - 21.557 \cdot C + 1540.9 \cdot C^2 - 194.7 \cdot C^3 \quad (9)$$

where:
C is the concentration of ammonia. In the application of Equation 7 the temperature must be given in *K* and the pressure in kPa.

d) The heat rate due to the fuel burning (heat of combustion), is given by Equation 10:

$$\dot{Q}_{fuel} = \dot{m}_{eg} \cdot LHV_{fuel} \quad (10)$$

where:
$\dot{Q}_{fuel}$ is the heat rate released from burning;
$\dot{m}_{eg}$ is the mass flow rate of the gases resulting from combustion and;
LHV_{fuel} is the lower calorific power of fuel.

Implementing the model in the steady state regime was divided into two parts: first, where the heat supplied by the fuel burned is determined, and second, thermodynamic modeling. In addition to the simplifying hypotheses presented above, the ammonia-water solution is considered to be a saturated liquid in points of state presented in Figure 2: 2 (COND outlet), 9 (SP inlet) and 16 (return of solution from RET to GERA); and saturated vapor at the following points: 1 (RET outlet), 6 (EVA outlet) and 15 (RET inlet). The model was developed on the EES® platform, where the system was formed by the equations of material, concentration and energy balances, and the closing equations.

Results and discussion

This section presents a comparison between the numerical and experimental data so as to examine the consistency of the modeling results. The gaseous fuel considered in the present model was Natural Gas, Table 1. The initial conditions adopted in numerical simulation are presented in Table 2.

Table 1. Composition of Natural Gas used in the model.

Component	Formula	Volume (%)	Component	Formula	Volume (%)
Methane	CH_4	82.55	i-Butane	iC_4H_{10}	0.71
Ethane	C_2H_6	14.69	n-Butane	nC_4H_{10}	0.14
Propane	C_3H_8	1.80	Pentane	C_5H_{12}	0.23

Table 2. Initial conditions for the steady state condition.

Environmental Conditions		Cold Water System	
Ambient temperature (K)	300.15	Cold water inlet temperature (K)	285.15
Atmospheric pressure (kPa)	101.30	Cold water Outlet temperature (K)	280.15
Refrigeration System		Flow rate of cold water in the pump (kg s^{-1})	4.21
Evaporation temperature (K)	278.15	Ammonia-water Solution	
Differential pressure valve V1 (kPa)	150.00	Concentration of ammonia in condenser and evaporator % (kg kg^{-1})	99.80
Heat Rate		Concentration of strong solution of ammonia in generator % (kg kg^{-1})	40.00
Heat rate in generator (kJ s^{-1})	152.50		

The concentration of ammonia was estimated to be 99.8% (kg kg^{-1}) in the following control volumes: COND, HEC and EVA.

Comparison of the numerical results and the experimental data of the ARS

For comparison purposes, numerical simulations were performed considering the operational conditions of the ARS. The environmental temperature considered was 304.65 K and the evaporation temperature was the same as that observed in the test, i.e. 281.85 K. Table 3 presents the results obtained for the analysis of the ROBUR® ARS. Where, *P* represented the state points from Figure 2, $Temp_{sim}$ represented the simulated temperature and the $Temp_{test}$ represented the experimental temperatures measures on the test bench.

The following conclusions can be drawn from Table 3: 1) the points with the lowest deviation are 3, 5, 8, 9 and 10, which correspond to the VR1, VR2, ABS, AHEA and SP outlets, respectively. The range between 1 and 5% are the points: 2, 6, 13 and 16, which correspond to the COND outlet, EVA outlet, RV3 inlet and solution return line from RET to GERA, respectively. On grouping the two intervals mentioned above, note that the streams comprising 3, 8, 9 and 10 present a relatively small deviation, and such points include the VR1, ABS, AHEA and SP outlets. Within the range from 5 to 10% are points 1, 4, 7, 11 and 15, i.e., the RET outlet, RV2, ABS and CABS inlets and GERA outlet, respectively. The deviation observed at Point 5 is affected by the deviation of Point 4, which corresponds to the HEC outlet on the high pressure side. The points with deviations higher than 10% are 12 and 14, corresponding to the CABS outlet and ABS inlet, where the liquid comes from RV3.

Table 4 combines points that fall within a certain range of bias, and by using this procedure, it can be verified in which regions the model of the present study provides more differences from the experimental data. The deviations presented by these points are caused by the difficulty in modeling the component, since inside ABS there is a mixture of solutions with internal heat generation.

Table 3. Comparison of temperatures obtained in the ARS simulation, with data obtained when testing the ROBUR® ARS. Initial data: environmental temperature of 304.65 K and evaporating temperature of 281.85 K.

P	Temp. sim. [K]	Temperature test [K]			Deviation [%]	P	Temp. sim. [K]	Temperature test [K]			Deviation [%]
		Minimum	Maximum	Average				Minimum	Maximum	Average	
1	330.42	346.35	350.51	348.43	5.17	9	314.65	309.91	317.28	313.60	0.34
2	314.65	309.88	312.48	311.18	1.12	10	314.85	313.21	317.38	315.30	0.14
3	311.16	308.78	311.84	310.31	0.27	11	320.70	337.43	349.1	343.27	6.57
4	283.54	298.03	303.29	300.66	5.69	12	337.50	376.60	381.20	378.90	10.93
5	280.31	279.86	283.39	281.63	0.47	13	380.45	394.77	404.24	399.51	4.77
6	281.85	282.11	289.59	285.85	1.40	14	349.33	393.16	403.24	398.20	12.27
7	306.18	283.21	288.22	285.72	7.16	15	355.03	375.72	382.93	379.33	6.40
8	340.58	336.23	347.37	341.80	0.36	16	355.14	355.49	376.84	366.17	3.01

Table 4. Grouping of the percentage deviations by frequencies.

Percentage bias [%]		Points	Frequencies
0	—	1	3, 5, 8, 9, 10	5
1	—	5	2, 6, 13, 16	4
5	—	10	1, 4, 7, 11, 15	5
	>	10	12, 14	2

From the analysis of Table 3, it can be observed that some values of the simulations are reasonably close to the average values acquired from the tests. The best agreement between test and simulation was obtained at Point 3, located between SP outlet and CRET inlet, as shown in Figure 2. The absolute deviation was only 0.14%. The point with the highest deviation was the fourteenth, between the RV3 outlet and ABS inlet, which reached a value of 12.27%.

Consistency examination of the results of the steady state modeling of the ARS

Having implemented the initial conditions presented in Table 1 and taking into consideration the simplifying assumptions of the eighteen points of state, the values of temperature, pressure, concentration and specific enthalpy were calculated (Table 5).

Table 5. State points with the parameters obtained in steady state simulation.

Point of State	Temperature (K)	Pressure (kPa)	Concentration of NH_3 (%, kg kg^{-1})	Specific Enthalpy (kJ kg^{-1})
1	327.42	1,428.00	99.86	1,340.00
2	310.15	1,428.00	99.80	1,747.00
3	306.29	1,278.00	99.80	1,747.00
4	280.62	1,278.00	99.80	33.52
5	276.66	478.80	99.80	33.52
6	278.15	478.80	99.80	1,276.00
7	303.60	478.80	99.80	1,340.00
8	335.59	478.80	51.28	390.60
9	310.15	478.80	51.28	-73.59
10	310.32	1,428.00	51.28	-72.05
11	315.46	1,428.00	51.28	-48.92
12	333.02	1,428.00	51.28	30.77
13	374.65	1,428.00	37.96	231.40
14	344.28	478.80	37.96	231.40
15	349.3	1,428.00	98.90	1,420.00
16	349.40	1,428.00	51.21	106.50

Notice that, in Table 5, the ARS has three levels of pressure: 478.80, 1,278.00 and 1,428.00 kPa. The smallest concentration of ammonia, 37.96%, was observed at state Points 13 and 14, which correspond to the outlet of the GERA and the outlet of the RV3, respectively. State point 16 (return of the solution rectified to GERA) presented an ammonia concentration of 51.21%, characterizing a condensation of ammonia together with the water. It is interesting to notice the temperature rise at the ABS outlet (point 8) at 335.59 K, as well as with the mixture of two flow rates with temperatures of 303.60 K at Point 7 with the solution coming from the HEC, and 344.28 K in point 14 where the solution comes from RV3.

Table 6 presents all heat rates of the equipment. In this table, GERA and EVA receive heat and COND and AHEA reject it. Table 7 shows the energy recovered in the RET and ABS coils and in HEC. Table 6 and 7 indicate that the total net heat exchanged in the absorption process is 179.49 kW (due to 153.20 + 26.29 kW). As a matter of the fact, it is necessary to have more heat in GERA so as to evaporate ammonia in the solution.

Table 6. Heat transfer rates in ARS.

Control volume	Heat transfer rate (kW)
GERA	152.50
COND	-82.71
EVA	88.33
AHEA	-153.20

Table 7. Heat in internal heat recovery in the ARS.

Control volume	Heat transfer rate (kW)
CRET	7.63
CABS	26.29
HEC	4.75

Figure 4 presents the Duhring diagram, wherein the logarithm of the pressure is plotted versus the negative reciprocal of the temperature (Herold et al., 1996), where the whole ARS cycle can be contemplated. Three pressure levels of the system are shown, where; P_H represents the higher level, P_I is the intermediate level and P_B the lower level of pressure.

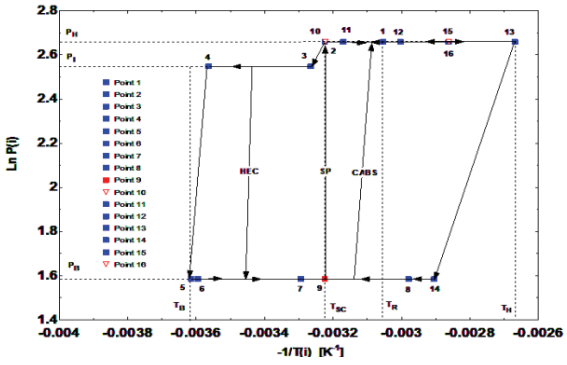

Figure 4. Duhring diagram for ambient temperature of 300.15 K and pressure in kPa.

Maximum and minimum temperatures are designated by T_H and T_B, while T_R is the outlet temperature of RET, and T_{SC} is the outlet temperature of COND. The arrows indicate the direction of the flow of the solution, where Points 13, 14 and 16 represent the flow of weak solution. Points 8, 9, 10, 11 and 12 refer to the flow of strong solution, and Points 1 to 7 refer to the rich solution flow where the ammonia concentration is 99.8% (kg kg^{-1}).

The Duhring diagram can indicate where the internal heat recovery may be necessary. In this

system, internal heat recovery occurs in RET, ABS and in HEC. The internal heat recovery in ABS is indicated by the arrow CABS and, shows the heat exchange from the absorber (Points 7 and 14) to the CABS (Points 11 and 12), and as a result, there was an increase of temperature in point 12 (CABS outlet). Another internal heat recovery is observed in HEC, where heat is exchanged from Points 3 and 4 to Points 6 and 7. With this heat gain at Point 6, the solution changes from a saturated vapor state to superheated vapor at Point 7. The internal heat recovery in the RET is not easy to visualize because it occurs at the same pressure level (1,428.00 kPa). The process where the solution moves from the low pressure to the high pressure (Points 9 and 10) is designated by the arrow related to the pumping process.

Figure 5 shows a correlation of enthalpy vs. mass fraction of ammonia for a binary mixture of ammonia and water. The solution enters the GERA at Point 12 as a subcooled liquid (solution with 51.28% of NH_3 concentration), whereas at Point 16 it enters as a saturated liquid state (a solution with a high concentration of water, 48.79%). At Point 13, the solution in the GERA outlet is a saturated liquid with a low level of NH_3 (poor solution, NH_3 at 37.96%). At Point 15, the solution from GERA is a saturated vapor (rich solution, NH_3 at 98.90%). The CRET is accommodated within the RET so Points 10 and 11 are part of this control volume. The state of Point 10 (at the coil inlet) is a subcooled liquid, with a concentration of 51.28% and at Point 11 (coil outlet) is in the same state.

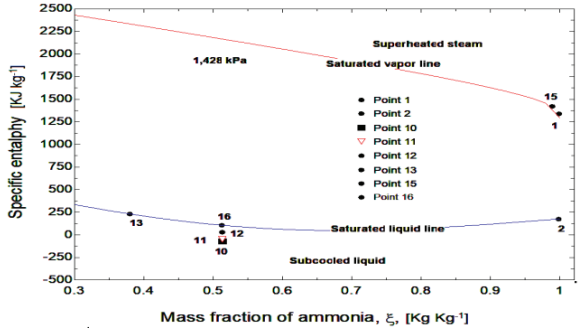

Figure 5. Ammonia-water solution behavior. Pressure of 1,428.00 kPa.

The COND control volume includes Points 1 and 2. Heat is expelled from the system, resulting in a change of thermodynamic state (Points 1 and 2). At Point 1, the solution is superheated and after losing sensible and latent heat, it becomes a saturated liquid at Point 2. Figure 6 presents the state points related to the RV1 control volume (Points 2 and 3). The first pressure drop can be observed, in State 2, where the solution is a saturated liquid and goes to the wet condition with a quality of 1.67% at Point 3.

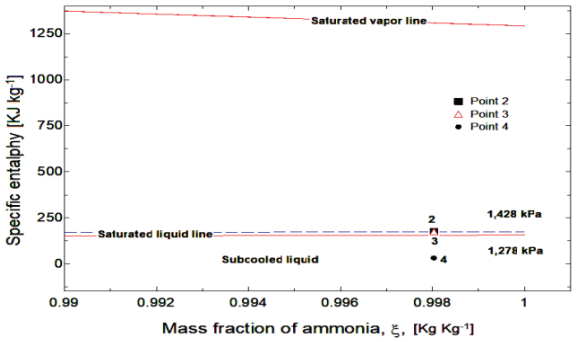

Figure 6. Ammonia-water solution behavior. Pressures 1,278.00 and 1,428.00 kPa.

Figure 7 shows the control volume of the EVA (Points 5 and 6). State 5, where the solution is in the condition of wet vapor, receives part of latent heat from the fluid that is supposed to be cooled, becoming, therefore, a saturated vapor at Point 6. This Figure also represents the ABS control volume (Points 7, 8 and 14), and these are superheated steam and stream with low quality (8.91%), respectively, when mixed to provide one flow of wet steam, at point 8. Hence, it presents better quality (24.07%), and the ammonia concentration reaches 51.28%.

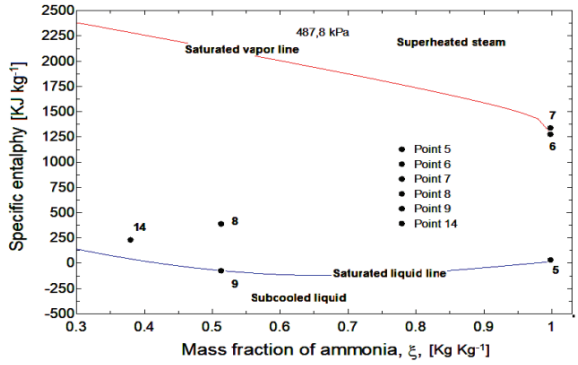

Figure 7. Ammonia-water solution behavior. Pressure: 478.80 kPa. Points of state at EVA, ABS and AHEA.

In this mixing process, heat is generated due to the solubility of ammonia in water, which causes the temperature of Point 8 to rise. Note that the absorption process in ABS has just begun at this point, and is completed in the AHEA (Points 8 and 9), and the heat of mixture is expelled into the environment. At state Point 8, the solution is in the region of wet steam and after the cooling process, reaches state Point 9, as a solution of saturated liquid.

Finally, Figure 8 represents the pumping process. The pressure of the solution is raised from 478.80 to 1,428.00 kPa, where the state Points 9 and 10 describe this operation.

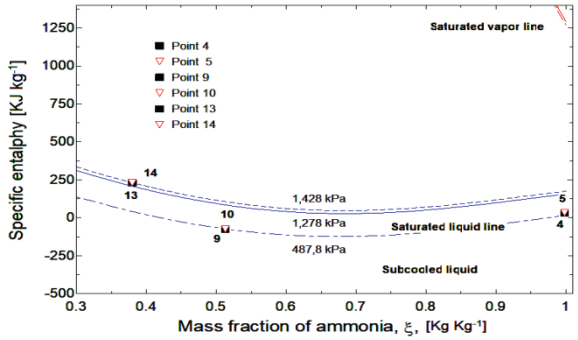

Figure 8. Ammonia-water behavior solution for two pressure levels. Emphasis is given to the state points SP with 9 and 10 and VR2 with points 4 and 5.

Figure 8 also presents, the control volume of VR3 (Points 13-14). In state Point 13, the solution is a saturated liquid, at a pressure of 1,428.00 kPa, and after throttling at Point 14, the solution drifts to the state of wet steam with a quality of 8.91% at a pressure of 478.80 kPa.

The coefficient of performance (COP) for the system for the present study was calculated as 0.5672, which is good, and in accordance with data from the open literature.

Conclusion

An absorption refrigeration system has been tested, modeled and simulated in the steady state regime based on the absorption chiller produced by ROBUR®, with 17.50 kW cooling capacity. Modeling was developed by using mass, concentration and energy balances in several points of the apparatus assembled for the tests.

Comparing the data obtained with simulations and the results collected during the tests, differences were observed between them. The point that presented the lowest percentage deviation was the CRET inlet, with 0.14%. The point of the greatest percentage deviation is located between the RV3 outlet and the ABS inlet, with 12.27%.

Acknowledgements

The completion of this work was only possible with the support from the following Institutions: *Conselho Nacional de Desenvolvimento Científico e Tecnológico* – CNPq (financial contribution), Federal University of Paraíba, University of Fortaleza and Federal University of Ceara, to which the authors are grateful. The penultimate author would like to thank the Facepe/Cnpq for financial support for research project APQ-0151-3.05/14. Moreover, the authors are also grateful to CAPES/UFPE/UFPB/URV for the partial financial support given to research project process: PVE 88881.030441/2013-01.

References

Amaris, C., Bourouis, M., Vallès, M., Salavera, D., & Coronas, A. (2014). Thermophysical properties and heat and mass transfer of new working fluids in plate heat exchangers for absorption refrigeration systems. *Heat Transfer Engineering, 36*(4), 388-395.

Beccali, M., Cellura, M., Longo, S., Nocke, B., & Finocchiaro, P. (2012). LCA of a solar heating and cooling system equipped with a small water–ammonia absorption chiller. *Solar Energy, 86*(5), 1491-1503.

Boudéhenn, F., Demasles, H., Wyttenbach, J., Jobard, X., Chèze, D., & Papillon, P. (2012). Development of a 5 kW cooling capacity ammonia-water absorption chiller for solar cooling applications. *Energy Procedia, 30*(1), 35-43.

Bourseau, P., & Bugarel, R. (1986). Absorption-diffusion machines: comparison of the performance of NH_3-H_2O and NH_3-NaSCN. *International Journal of Refrigeration, 9*(4), 206-214.

Darwish, N. A., Al-Hashimi, S. H., & Al-Mansoori, A. S. (2008). Performance analysis, evaluation of a commercial absorption-refrigeration water-ammonia (ARWA) system. *International Journal of Refrigeration, 31*(7), 1214-1223.

Edem, N. T. K., Le Pierrès, N., & Luo, L. (2012). Numerical dynamic simulation and analysis of a lithium bromide - water long-term solar heat storage system. *Energy, 37*(1), 346-358.

Herold, K. E., Radermacher, R., & Klein, S. A. (1996). *Absorption chillers and heat pumps*. Boca Raton, FL: CRC Press LLC.

Kim, B., & Park, J. (2007). Dynamic simulation of a single-effect ammonia-water absorption chiller. *International Journal of Refrigeration, 30*(3), 535-545.

Kohlenbach, P., & Ziegler, F. (2008a). A dynamic simulation model for transient absorption chiller performance. Part I: The model. *International Journal of Refrigeration, 31*(2), 217-225.

Kohlenbach, P., & Ziegler, F. (2008b). A dynamic simulation model for transient absorption chiller performance. Part II: Numerical results and experimental verification. *International Journal of Refrigeration, 31*(2), 226-233.

Le Lostec, B., Galanis, N., & Millette, J. (2012). Experimental study of an ammonia-water absorption chiller. *International Journal of Refrigeration, 35*(8), 2275-2286.

Le Lostec, B., Galanis, N., & Millette, J. (2013). Simulation of an ammonia–water absorption chiller. *Renewable Energy, 60*(1), 269-283.

Libotean, S., Salavera, D., Valles, M., Esteve, X., & Coronas, A. (2007). Vapor−liquid equilibrium of ammonia+lithium nitrate + water and ammonia + lithium nitrate solutions from (293.15 to 353.15) K. *Journal of Chemical and Engineering Data, 52*(3), 1050-1055.

Lin, P., Wang, R. Z., & Xia, Z. Z. (2011). Numerical investigation of a two-stage air-cooled absorption refrigeration system for solar cooling: Cycle analysis and absorption cooling performances. *Renewable Energy, 36*(5), 1401-1412.

Moya, M., Bruno, J. C., Eguia, P., Torres, E., Zamora, I., & Coronas, A. (2011). Performance analysis of a trigeneration system based on a micro gas turbine and an air-cooled, indirect fired, ammonia-water absorption chiller. *Applied Energy, 88*(12), 4424-4440.

Ochoa, A. A. V., Dutra, J. C. C., & Henríquez, J. R. G. (2014). Energy and exergy analysis of the performance of 10 TR lithium bromide/water absorption chiller. *Revista Técnica de la Facultad de Ingeniería, 37*(1), 38-47.

Ochoa, A. A. V., Dutra, J. C. C., Henríquez, J. R. G., & Rohatgi, J. (2014). Energetic and exergetic study of a 10RT absorption chiller integrated into a microgeneration system. *Energy Conversion and Management, 88*(1), 545-553.

Ochoa, A. A. V., Dutra, J. C. C., Henríquez, J. R. G., & Santos, C. A. C. (2016). Dynamic study of a single effect absorption chiller using the pair LiBr/H_2O. *Energy Conversion and Management, 108*(1), 30-42.

Ozgoren, M., Bilgili, M., & Babayigit, O. (2012). Hourly performance prediction of ammonia - water solar absorption refrigeration. *Applied Thermal Engineering, 40*(1), 80-90.

Pratihar, A. K., Kaushik, S. C., & Agarwal, R. S. (2012). Performance evaluation of a small capacity compression/absorption refrigeration system. *Applied Thermal Engineering, 42*(1), 41-48.

Rabah, G. (2010). Investigation of the potential of application of single effect and multiple effect absorption cooling systems. *Energy Conversion and Management, 51*(1), 1629-1636.

Rivera, W., Best, R., Cardoso, M. J., & Romero, R. J. (2015). A review of absorption heat transformer. *Applied Thermal Engineering, 91*(1), 654-670.

Rodriguez-Muñoz, J. L., & Belman-Flores, J. M. (2014). Review of diffusion–absorption refrigeration technologies. *Renewable and Sustainable Energy Reviews, 30*(1), 145-153.

Said, S. A. M., Spindler, K., El-Shaarawi, M. A., Siddiqui, M. U., Schmid, F., Bierling, B., & Khan, M. M. A. (2015). Design, construction and operation of a solar powered ammonia-water absorption refrigeration system in Saudi Arabia. *International Journal of Refrigeration, 62*(1), 222-231.

Somers, C., Mortazavi, A., Hwang, Y., Radermacher, R., Rodgers, P., & Al-Hashimi, P. (2011). Modeling water/lithium bromide absorption chillers in ASPEN Plus. *Applied Energy, 88*(11), 4197-4205.

Wu, T., Wu, Y., Yu, Z., Zhao, H., & Wu, H. (2011). Experimental investigation on an ammonia–water–lithium bromide absorption refrigeration system without solution pump. *Energy Conversion and Management, 52*(1), 2314-2319.

Wu, W., Shi, W., Li, X., & Wang, B. (2015). Air source absorption heat pump in district heating: Applicability analysis and improvement options. *Energy Conversion and Management, 96*(1), 197-207.

Wu, W., Wang, B., Shi, W., & Li, X. (2014). An overview of ammonia-based absorption chillers and heat pumps. *Renewable and Sustainable Energy Reviews, 31*(1), 681-707.

Zotter, G., & Rieberer, R. (2015). Experimental analysis of a novel concept of a "thermally driven" solution pump operating a small-capacity ammonia/water absorption heat pumping system. *International Journal of Refrigeration, 60*(1), 190-205.

Received on November 22, 2015.
Accepted on June 8, 2016.